Hindawi
Advances in Materials Science and Engineering
Volume 2019, Article ID 1567824, 14 pages
https://doi.org/10.1155/2019/1567824

Research Article

Sol-Gel Synthesis of TiO_2 Nanocrystalline Particles with Enhanced Surface Area through the Reverse Micelle Approach

Mohammad Hossein Nateq and Riccardo Ceccato

Department of Industrial Engineering, University of Trento, Via Sommarive 9, 38123 Trento, Italy

Correspondence should be addressed to Mohammad Hossein Nateq; mohammadhosein.nateq@unitn.it

Received 22 July 2019; Revised 25 September 2019; Accepted 1 October 2019; Published 11 November 2019

Academic Editor: Marinos Pitsikalis

Titania nanocrystalline particles were synthesized by hydrolysis-condensation of titanium tetraisopropoxide in water-in-oil micellar solutions of water/cyclohexane/Triton X-100 system, and the effects of reflux time and water-to-surfactant molar ratio on the particle uniformity, crystallinity, and surface area were studied. Several characterization techniques including TEM and SEM, as well as X-ray diffraction and FT-IR spectroscopy, helium pycnometry, and nitrogen physisorption, were employed to evaluate the particle density and dimensions, crystallite size, surface area value, and the porosity features in the as-prepared condition and also after thermal treatment at 500°C. The results show that all treated samples are dense nanocrystalline anatase particles with BET surface area values over 100 $m^2 \cdot g^{-1}$ and primary particle size of 10–15 nm. However, for the as-prepared samples, as the reflux time increases, a better purification of particles from the synthesis environment is resulted, leading to denser and more crystalline powders with smaller particle size and higher BET surface area values culminating in 179 $m^2 \cdot g^{-1}$ for 24 hours of refluxing. Moreover, decreasing the water-to-surfactant molar ratio from 10 to 5 and 2 increases the particles surface area to 239 and 224 $m^2 \cdot g^{-1}$, respectively, at the expense of slight density and crystallinity degradation and considerable prolongation of surfactant removal step. Supportively, the comparison between photocatalytic activities of as-prepared samples also evidences the effectiveness of reflux time extension on improving the sample features and enhancing their functionality. This study can highlight how the earlier synthesis steps can influence the evolution of the structure of the final products.

1. Introduction

TiO_2 nanostructures are highly functional materials for solar energy conversion applications such as photocatalysis and photovoltaics owing to the superior optoelectrical properties and outstanding chemical stability [1, 2]. The results of previous investigations indicate that the solar energy conversion efficiency of the photovoltaic devices utilizing nanocrystalline TiO_2 is critically dependent on the phase, morphology, and porosity features of the titania [3–6]. For example, in dye-sensitized solar cells (DSSCs), narrow size distributed mesoporous anatase nanoparticles with high values of surface area and pore volume are known to be much more effective in improving the charge transfer properties as well as providing sufficient dye absorption capacity and enough volume for the electrolyte diffusion, which ultimately result in enhanced energy conversion efficiency and superior performance [7, 8].

The sol-gel synthesis has been successfully applied for preparing nanocrystalline metallic oxide materials including TiO_2. In general, this method involves the hydrolysis and condensation of a metal alkoxide such as titanium(IV) isopropoxide and yielding intermediate oxo-hydroxide spices which eventually form the metal oxide [1, 9, 10]. However, precise controlling of hydrolysis step through adjusting the sol pH and temperature is critically essential to obtain homogeneous nanoscale oxide networks [4]. Moreover, the as-synthesized precipitates are generally amorphous and a postcalcination temperature over 300°C is required to obtain the anatase phase, whereby the inevitable particle enlargement due to the agglomeration causes collapse of the pore structure and surface area reduction [11].

Consequently, although sol-gel synthesis routes are capable of large-scale production of TiO_2 nanoparticles with high surface area, limitations still exist, including particle aggregation and wide distribution of particle size [3].

A better control on the shape uniformity, size distribution, and crystallinity of nanoparticles can be obtained through the surfactant-mediated sol-gel route by employing the reverse micelles [11–14]. This method provides a controlled synthesis approach whereby the hydrolysis of the precursor is confined to the nanodroplets of water which are previously trapped and stabilized in a dry organic nonpolar solvent through a shell of surfactant molecules separating the polar and the nonpolar domains. The thermodynamic stability of such a system containing two immiscible liquids is by the virtue of the amphiphilic nature of surfactant molecules, whereby the hydrophilic heads of the molecules cover the surface of water nanodroplets while the hydrophobic tails align outwards in the nonpolar solvent. The subsequent reduction in the interfacial free energy results in the spontaneous formation of water nanodroplets dispersed in the nonpolar solvent. These monodispersed spherical surfactant-covered water pools, called reverse micelles, provide excellent reaction sites for the formation of nanoparticles as the surfactant shell acts as a surface agent, limiting the future growth, and prevents the particles from aggregation and coalescence [15–17]. Besides, this method impedes the precipitation of metal hydroxide due to probable uncontrolled hydrolysis and condensation of the alkoxide, which leads to the formation of heterogeneous nucleation sites and therefore generation of large clusters with broad size distributions [18].

The synthesis of TiO_2 nanoparticles via the reverse micelle method involves three stages: (1) formation of a water-in-oil microemulsion environment as the reverse micelles in the water/solvent/surfactant system; (2) adding the alkoxide precursor solution such as titanium(IV) tetraisopropoxide to trigger the hydrolysis reaction in the reverse micellar environment and formation of nanoscale TiO_2 network; and (3) washing or removal of the surfactant from the system to obtain the nanocrystalline powders. Several factors determine the final features of the obtained nanoparticles, among which the choice of the surfactant is the fundamental one. Different types of surfactant including AOT [19, 20] and SDS [21] as anionic surfactants and also Brij and Tween series [22] as well as Triton X-100 [23–25] as the nonionic ones have been employed for the surfactant-mediated sol-gel synthesis of TiO_2. The results show that, in addition, to affect the shape and morphology of nanoparticles, the surfactant structure plays a decisive role in all synthesis stages. The quality of the gel and the subsequent nanoparticles strongly depends on the kinetics of the hydrolysis step [11, 23]. Upon the addition of TTIP solution to the reverse micelle environment, the surfactant layer is the barrier against the alkoxide hydrolysis; however, the microemulsion is a dynamic system and the surfactants involved in the formation of the layers repeatedly leave the micelles and are replaced by others that freely move in the solvent [14], providing the exchange of materials throughout the barrier with the so-called intermicellar exchange rate. Thereafter, the nucleation initially begins on the micelle edges and continues inwards with the arrival of more TTIP fed via the intermicellar exchange [15]. So the barrier that determines the intermicellar exchange rate and thus the kinetics of the hydrolysis step depends on the rigidity of the micelle interface [15]. In a microemulsion system with a high interfacial rigidity, formation of more stable water pools leads to obtaining nanoparticles with smaller crystallite size and narrow size distributions due to the gradual hydrolysis of titanium alkoxide [11, 23]. A surfactant with a longer hydrocarbon chain can prohibit accessing the water inside the micelles more effectively whereby the interfacial rigidity increases. Besides, a lower area per molecule adopted by the surfactant leads to a higher packing density of the interfacial film and thus a higher rigidity [12, 15]. In addition to the hydrolysis part, the last step involving the removal of surfactant molecules from the gel significantly affects the final product quality as well since the remaining organic molecules degrade the nanoparticle surface properties. Here, nonionic surfactants provide better applicability owing to easier removal procedure compared to the ionic and cationic ones [26]. Triton X-100, a polyoxyethylene derivative, is a nonionic surfactant of nearly 50 square angstroms surface area with a hydrophilic chain containing an average of 9.5 ethylene oxide units, which is longer than the lipophilic part made of an aromatic hydrocarbon chain [27]. Having such properties, Triton X-100 is a promising candidate for template synthesis of nanoparticles via reverse micelle approach.

The other variant affecting the quality of synthesized nanoparticles is the molar ratio of initial compounds. Several studies [15–17] have shown an increase in particle size with increasing the precursor concentration. Moreover, since the volume of trapped water pools determines the reverse micelle radius, it is possible to control the size of nanoparticles through adjusting the molar ratio of the water to surfactant, S, as $W = [H_2O]/[S]$. Generally, decreasing the ratio leads to smaller water nanodroplets and consequently smaller particles [12, 15] which can be attributed to the effect of water structure inside the water pool on the interfacial layer rigidity. In a system with a low W ratio, the small number of water per surfactant molecules induces a strong interaction between water molecules and the hydrophilic heads of the surfactant, as almost all of the water molecules inside the water pools can be considered as "bound." This condition leads to a high interfacial rigidity, thereby slowing down the intermicellar exchange, and low growth rate. On the contrary, with a higher W ratio, the volume of water nanodroplets increases, whereby the condition for a portion of water molecules changes from "bound" to "free" state, resulting less stable water pools and accelerated intermicellar exchange and fast growth rate [15, 16].

In addition to the high value of the surface area, shape uniformity, and narrow size distribution, the higher crystallinity of the as-prepared powder is considered as another factor defining the nanoparticle quality. Owing to lower density of trap states and thus smaller recombination rates of photoexcited electrons [28], the photocatalytic activity of TiO_2 nanoparticles is strongly enhanced by increasing the

crystallinity which could be achieved through a high-temperature thermal treatment. However, due to the agglomeration of nanoparticles during the postcalcination treatment and the subsequent collapse of the pore structure and surface area reduction, preparing highly crystalline as-prepared TiO_2 nanoparticle without further requirement for high-temperature crystallization is particularly favoured [11]. As a logical extrapolation, refluxing the solvent at temperatures considerably lower than those required for the traditional calcination process may be able to crystallize the amorphous nanoparticles synthesized and encapsulated in micellar cavities without significant damage to the micellar structures.

In this paper, we investigate the effects of water-to-surfactant molar ratio, W, and the refluxing time, R, on the surface area, porosity features, and crystallite size of TiO_2 nanoparticles synthesized through the reverse micelle method in water/cyclohexane/Triton X-100 system with the particular scope of obtaining higher quality as-prepared nanoparticles in terms of enhanced photocatalytic functionality. Although the reverse micelle method has been studied extensively [11–25], to the best of our knowledge, obtaining crystalline as-prepared TiO_2 nanoparticles as a result of reflux time effect has not been investigated before; thus, the findings can contribute to synthesize TiO_2 nanoparticles of superior photocatalytic and photovoltaic performance.

2. Materials and Methods

2.1. Synthesis Procedure. Titanium(IV) isopropoxide (TTIP) (ABCR, Germany), cyclohexane (Cy), and Triton X-100® (TX) (Sigma-Aldrich, USA) were used as precursor, solvent, and surfactant, respectively, without further purification, and distilled water was applied to initiate the hydrolysis. All the amounts of the reagents were kept fixed to the following values, in molar ratios: $[H_2O]/[TX]/[TTIP] = 10/1/1$, whereas cyclohexane volumes were evaluated from the ratio: $[TTIP]/[Cy] = 5{\cdot}10^{-4}$ mol·ml^{-1}, as reported in the literature [29]. Figure 1 shows the schematic representation of the synthesis procedure. Firstly, the reverse micellar environment was prepared by the dissolution of TX in Cy at room temperature and stirring for 10 minutes and then the dropwise addition of stoichiometric amount of distilled water followed by a further 30 minutes stirring. In the next step, the solution of TTIP in Cy was added to the reverse micelle solution and immediately the powder formation occurred. All the obtained suspensions were left under stirring for 30 min before stopping the reaction (sample with no reflux) or starting the reflux step at 80°C for different times. Further step provided the removal of the micellar environment by adding to the suspensions a fixed volume of water/ethanol = 1/1 solution and leaving them in a separation funnel until the complete separation between oil and aqueous phases occurred. Then powders were filtered and washed 4 times with the same amount of water; a drying was performed on the powders at 80°C overnight. Obtained products were labelled as R_x samples, with $x = 0$, 1, 2, 15, and 24 representing the time, as hours, of the refluxing step of the suspension. Following similar synthesis procedure, two other samples were prepared with refluxing time of 24 h but employing different $W = [H_2O]/[TX]$ molar ratios of 5 and 2 instead of the previously used $W = 10$. These samples, labelled as W_5 and W_2, formed the second group of samples together with the W_{10} (R_{24}). Finally, a fraction of all samples were taken for heat treatment at 500°C for 2 h in a static air oven. Figure 1 summarizes the steps for preparation of TiO_2 nanoparticles.

2.2. Characterization. The as-prepared and treated powders were characterized by several techniques. Density measurements were performed by a Micromeritics 1035 helium pycnometer (Micromeritics, USA), and N_2 sorption isothermal analyses were obtained by a Micromeritics ASAP 2010 porosimeter (Micromeritics, USA). Before the analysis, each sample was degassed at a final pressure of <1.3 Pa. The assessment of their surface area values was performed by using BET equation, applied in the range: $0.05 < P/P_0 < 0.33$. Then the BJH model was applied in order to classify the pore size distribution curves. From the above data, primary particle dimensions were evaluated, under the assumption of a spherical symmetry, using the following equation:

$$d = \frac{6}{\mathrm{SSA} \cdot \rho}, \tag{1}$$

where d is the primary particle dimension, SSA means the specific surface area value, and ρ represents the skeletal density.

SEM micrographs were obtained by JSM-5500 instrument (JEOL, Japan), operating at a voltage of 10 kV. FT-IR measurements were performed on powders dispersed into KBr pellets using an Avatar 330 spectrophotometer (Thermo Nicolet, USA). TEM images, SAED patterns, and regarding indexing graphs were obtained using a STEM microscope, Talos™ F200S S/TEM instrument (Thermo Fisher, USA), operating under accelerating voltage of 200 kV. The XRD spectra were collected with a Rigaku IIID-Max powder diffractometer (Rigaku, Japan), employing Cu K$\alpha\alpha$1 radiation ($\lambda = 0.154056$ nm) and a graphite curved monochromator, set on the diffracted beam. Experimental spectra were evaluated, in terms of phase content and line profile analysis, by using MAUD software, a derived Rietveld method for quantitative analysis, associated with Warren–Averbach theory for the crystallite size evaluation [30].

2.3. Photocatalytic Tests. The photocatalytic activities of as-prepared samples were checked by the degradation of aqueous solutions of Calmagite dye (0.1 % weight; Sigma-Aldrich, USA). Typically, a fixed amount of as-prepared TiO_2 nanoparticles was added to the solution in a quartz cuvette; then, the solution was irradiated for 20 s by UV rays of $\lambda = 220$ nm wavelength using JASCO V-570 spectrophotometer (JASCO, Japan). After the UV irradiation, the wavelength was set at 528 nm in order to measure the decrease in absorbance of the purple-coloured dye solution as a function of time. The solution with no addition of nanoparticles was analysed with the same protocol as the blank test.

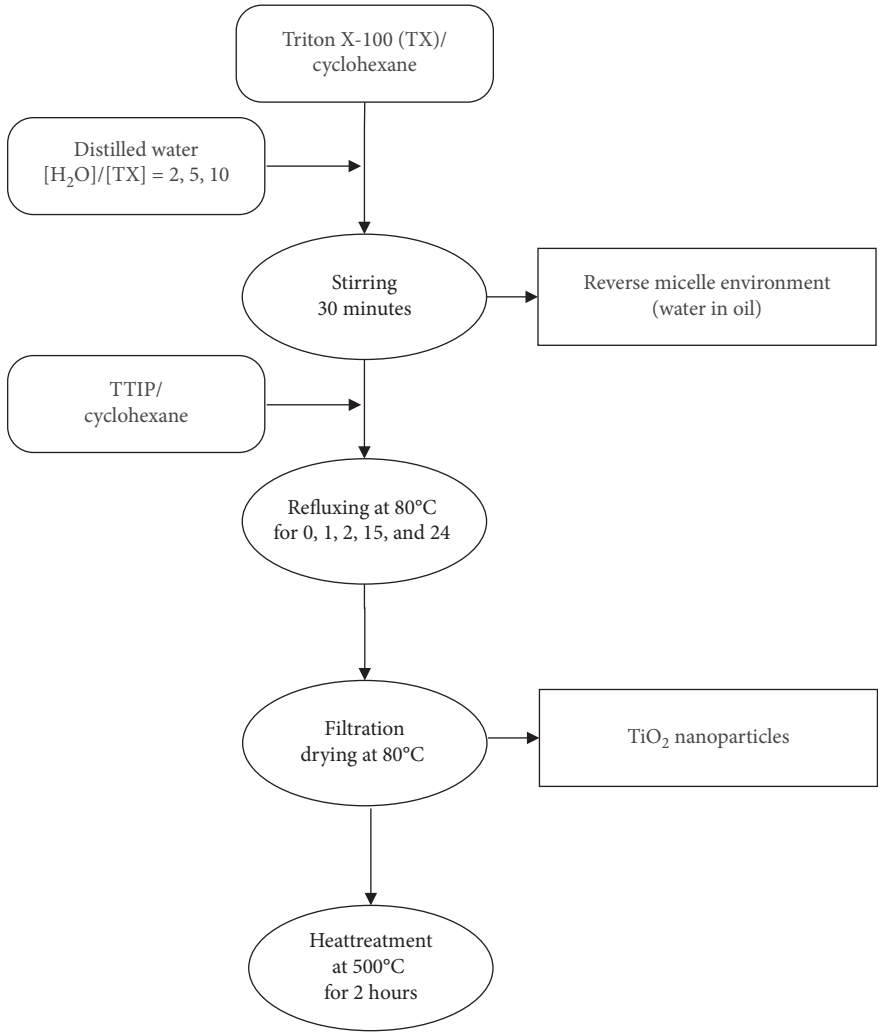

Figure 1: The flowchart summarizing the preparation steps of TiO_2 nanoparticles.

3. Results

The results of the X-ray diffraction analysis, helium pycnometry measurements, and also N_2 physisorption analysis are reported in Tables 1 and 2, regarding the as-prepared and treated powders, respectively. Figure 2 provides a visual comparison for as-prepared R_0 and R_{24} samples, followed by two pairs of high- and low-magnification SEM images. In Figure 3, for as-prepared powders synthesized through different refluxing times and W ratios, the FT-IR spectra are depicted, comparing all samples after being washed for four times. Moreover, for the as-prepared R_{24} sample, the FT-IR spectra after different numbers of washing are compared with the spectrum of the treated R_{24} sample. In Figure 4, the TEM images of R_{24} (W_{10}) and W_2 samples in as-prepared and treated conditions are shown in addition to regarding SAED patterns and indexing graphs, followed by X-ray diffraction patterns of all samples in Figure 5. The isothermal N_2 physisorption curves of the samples in the as-prepared and the treated condition are illustrated in Figure 6. The sample porosity features are reported in terms of the total pore volume and average pore diameter in Figure 7, as well as the pore size distribution and the modal pore diameter in Figure 8, respectively. Finally, the comparison between photocatalytic activities of as-prepared TiO_2 nanoparticles is shown in Figure 9 through depicting the relative absorbance degradation of the Calmagite dye solution over the time as a result of UV irradiation in the presence of the samples.

4. Discussion

4.1. As-Prepared Samples. The first goal of this work was to enhance the uniformity and crystallinity of the as-prepared TiO_2 nanoparticles as a function of the reflux time. The powder uniformity was studied in terms of skeletal density, particle dimension, and remaining surfactant amount, and the results of XRD analysis and TEM observation were used to investigate the powder crystallinity.

According to the values reported in Table 1 for as-prepared samples, as a general trend, the increase of the reflux time leads to higher values of the skeletal density together with the decrease of the particle dimensions. An indirect proof of this feature can be evidenced from SEM micrographs, reported in Figure 2 for the samples R_0 and R_{24}

Table 1: Structural and morphological parameters of the as-prepared TiO_2 samples.

Sample	Phase	Crystallite size (nm)	Density ($g \cdot cm^{-3}$)	BET surface area ($m^2 \cdot g^{-1}$)	Particle size[2] (nm)
R_0	Amorphous	n.e.[1]	1.840 ± 0.005	15.8 ± 0.9	205.4 ± 0.2
R_1	Amorphous	n.e.	1.803 ± 0.005	74.4 ± 0.3	37.9 ± 0.4
R_2	Anatase	4.1 ± 0.6	1.471 ± 0.001	34.5 ± 0.2	118.2 ± 0.7
R_{15}	Anatase	6.1 ± 0.3	2.173 ± 0.006	77.6 ± 0.6	35.6 ± 0.3
R_{24} (W_{10})	Anatase	6.3 ± 0.5	3.133 ± 0.006	178.8 ± 1	10.7 ± 0.6
W_5	Anatase	5.4 ± 0.4	3.180 ± 0.040	239.4 ± 3	7.9 ± 0.2
W_2	Anatase	4.6 ± 0.1	2.753 ± 0.005	224.6 ± 3	9.7 ± 0.4

[1]Not evaluable. [2]Calculated under the assumption of spherical symmetry according to equation (1).

Table 2: Structural and morphological parameters of the TiO_2 samples treated at 500°C for 1 h.

Sample	Phase	Crystallite size (nm)	Density ($g \cdot cm^{-3}$)	BET surface area ($m^2 \cdot g^{-1}$)	Particle size[2] (nm)
R_0	Anatase	15.3 ± 0.2	3.51 ± 0.02	101.6 ± 0.6	15.8 ± 0.1
R_1	Anatase	17 ± 2	3.51 ± 0.02	88.0 ± 0.5	22.9 ± 0.1
R_2	Anatase	15 ± 2	3.66 ± 0.02	104.6 ± 0.5	15.6 ± 0.1
R_{15}	Anatase[1]	15 ± 1	3.63 ± 0.02	116.0 ± 0.5	14.2 ± 0.1
R_{24} (W_{10})	Anatase[1]	13.6 ± 0.2	3.67 ± 0.01	123.1 ± 0.4	13.3 ± 0.1
W_5	Anatase	13.7 ± 0.2	3.75 ± 0.02	126.6 ± 0.7	12.9 ± 0.1
W_2	Anatase	13.4 ± 0.1	3.62 ± 0.06	121.2 ± 0.3	13.1 ± 0.1

[1]Some brookite phase is present (<5% weight). [2]Calculated under the assumption of spherical symmetry according to equation (1).

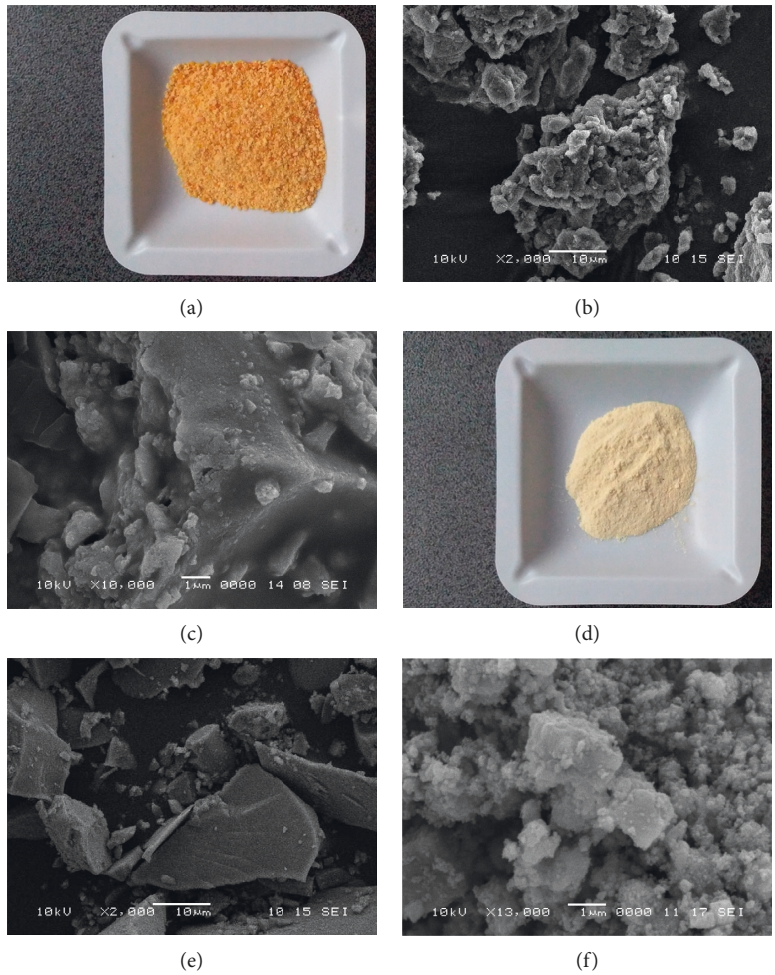

(a) (b) (c) (d) (e) (f)

Figure 2: The as-prepared R_0 sample (a) and its SEM images under low (b) and high magnifications (c) in comparison with the as-prepared R_{24} sample (d) and its SEM images under low (e) and high magnifications (f).

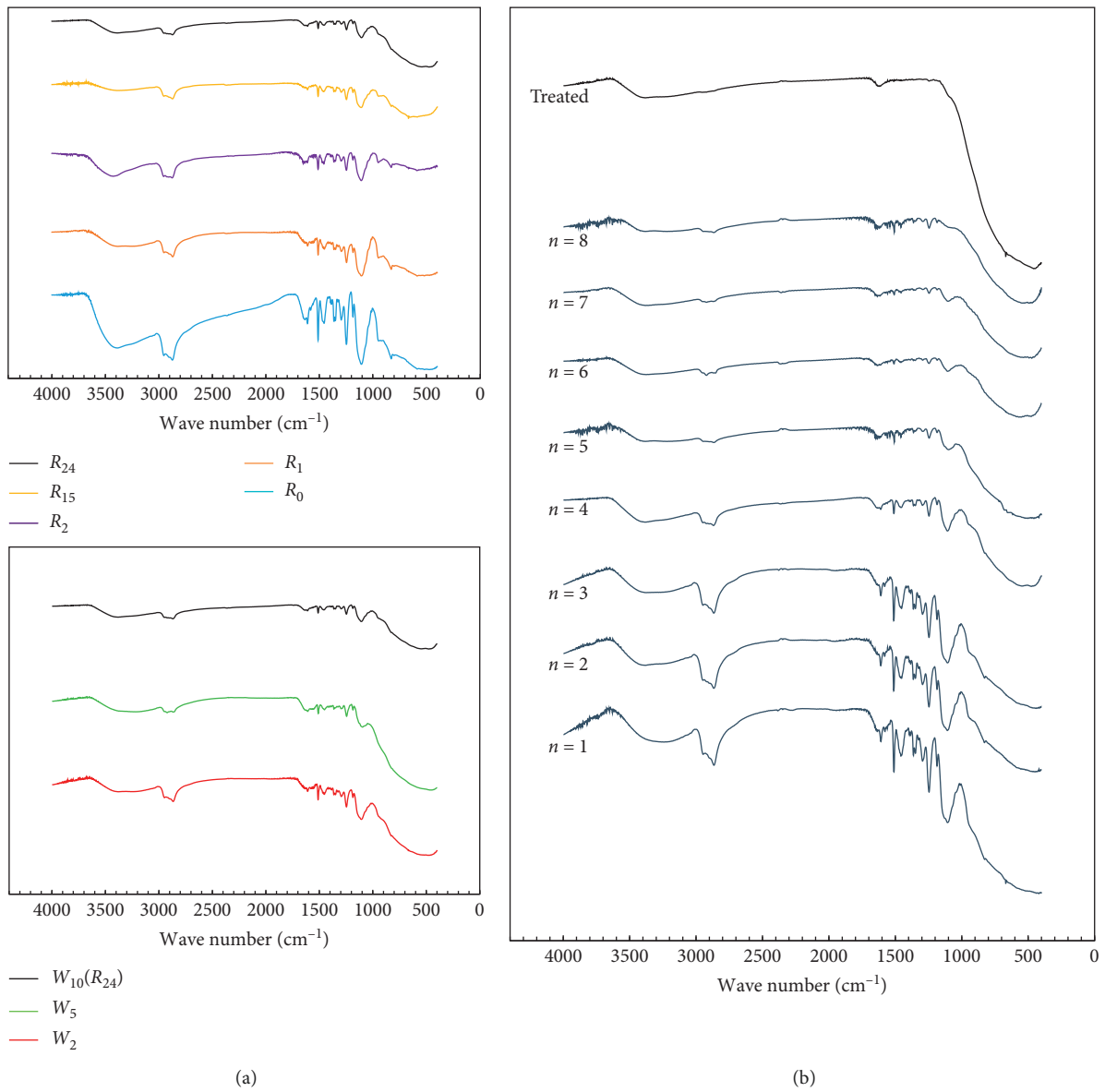

FIGURE 3: The FT-IR spectra of as-prepared powders synthesized through different refluxing times (upper part) and W ratios (lower part) after being washed for four times (a) and the FT-IR spectra of the as-prepared R_{24} sample after different numbers of washing ($n = 1$ to 8) compared with the spectrum of the treated R_{24} one (b).

comparatively. In low magnification, both samples look like large aggregates of primary particles while some differences could be observed in the high-magnification mode: the surface of the R_0 particles appears very smooth and flat, whereas the R_{24} particles look like more ordered with a prismatic symmetry. Seemingly, aggregates in R_0 are formed since the surfactant is still present, entrapped among the nanoparticles. The presence of –OH groups can act as specific sites for the aggregation of the primary particles afterwards. In Figure 3(a), the FT-IR spectra confirm that the surfactant is still present in as-prepared samples after four times of washing since the absorption peaks attributable to organic residuals are detected, including CH_2 and OH stretching peaks in the range of 2800 to 3000 cm^{-1} and 3000 to 3500 cm^{-1}, respectively. However, as the reflux time extends, the intensity of peaks turns out to be considerably small, indicating negligible surfactant contents in the samples R_{15} and R_{24}. Moreover, as shown in Figure 3(b) for the sample R_{24}, an almost surfactant-free product comparable with the treated sample is possible to obtain by increasing the numbers of washing. For the samples W_5 and W_2 that contained higher amounts of initial surfactant, more remained organic residuals are detected compared with the sample R_{24}, making the required numbers of washing up to nearly double to obtain an almost surfactant-free sample (not shown here). Thus, as the first result, it can be concluded that a sufficiently long reflux time brings about the capability of removing almost all contaminants and results in powders of smaller particle size and higher density while short refluxing times lead to formation of large particles of

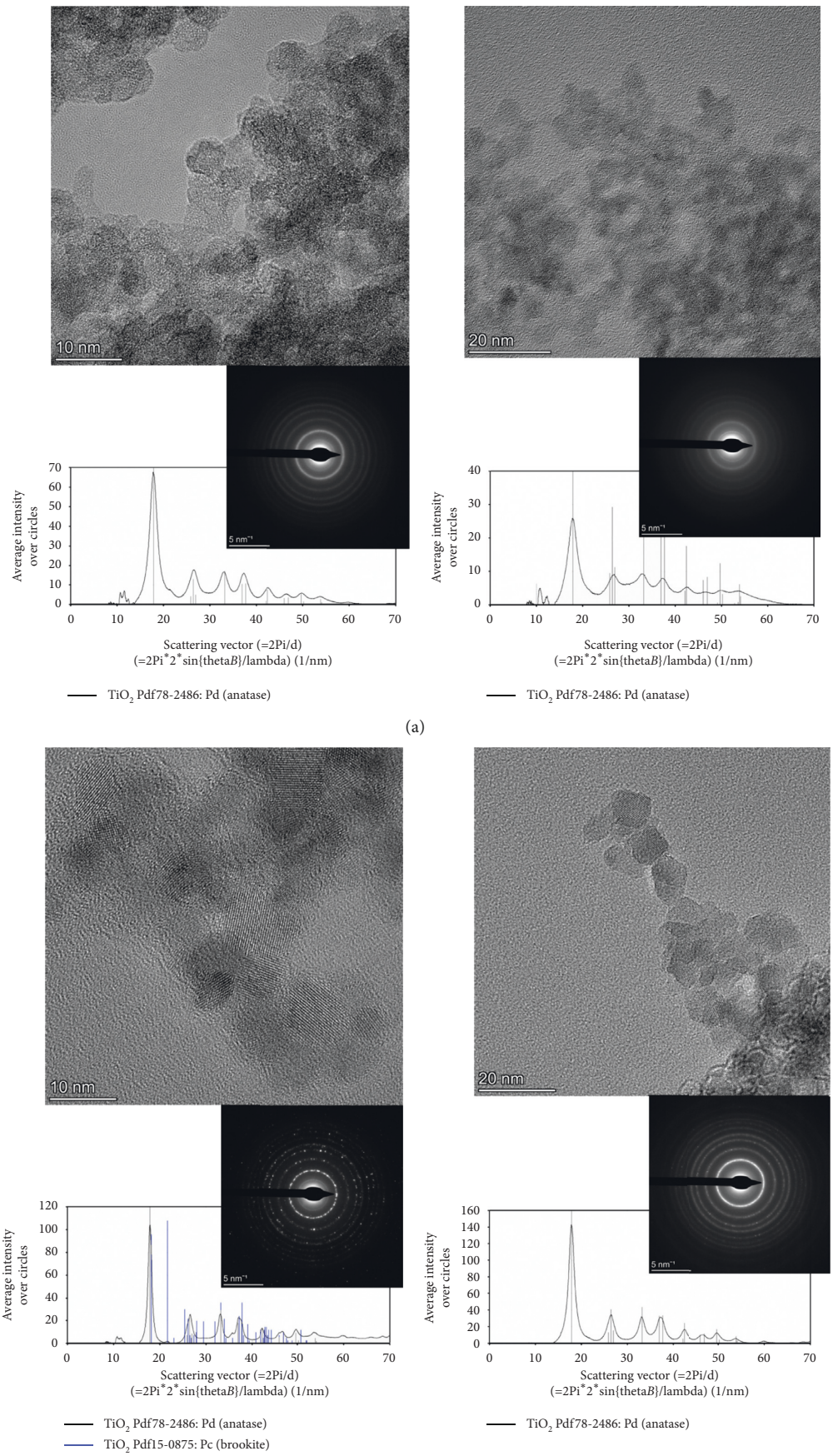

(a)

(b)

Figure 4: TEM images of TiO_2 nanoparticles in the as-prepared state (a) and treated condition (b), in addition to regarding SAED patterns and indexing graphs for the samples R_{24} (W_{10})(on the left) and W_2 (on the right).

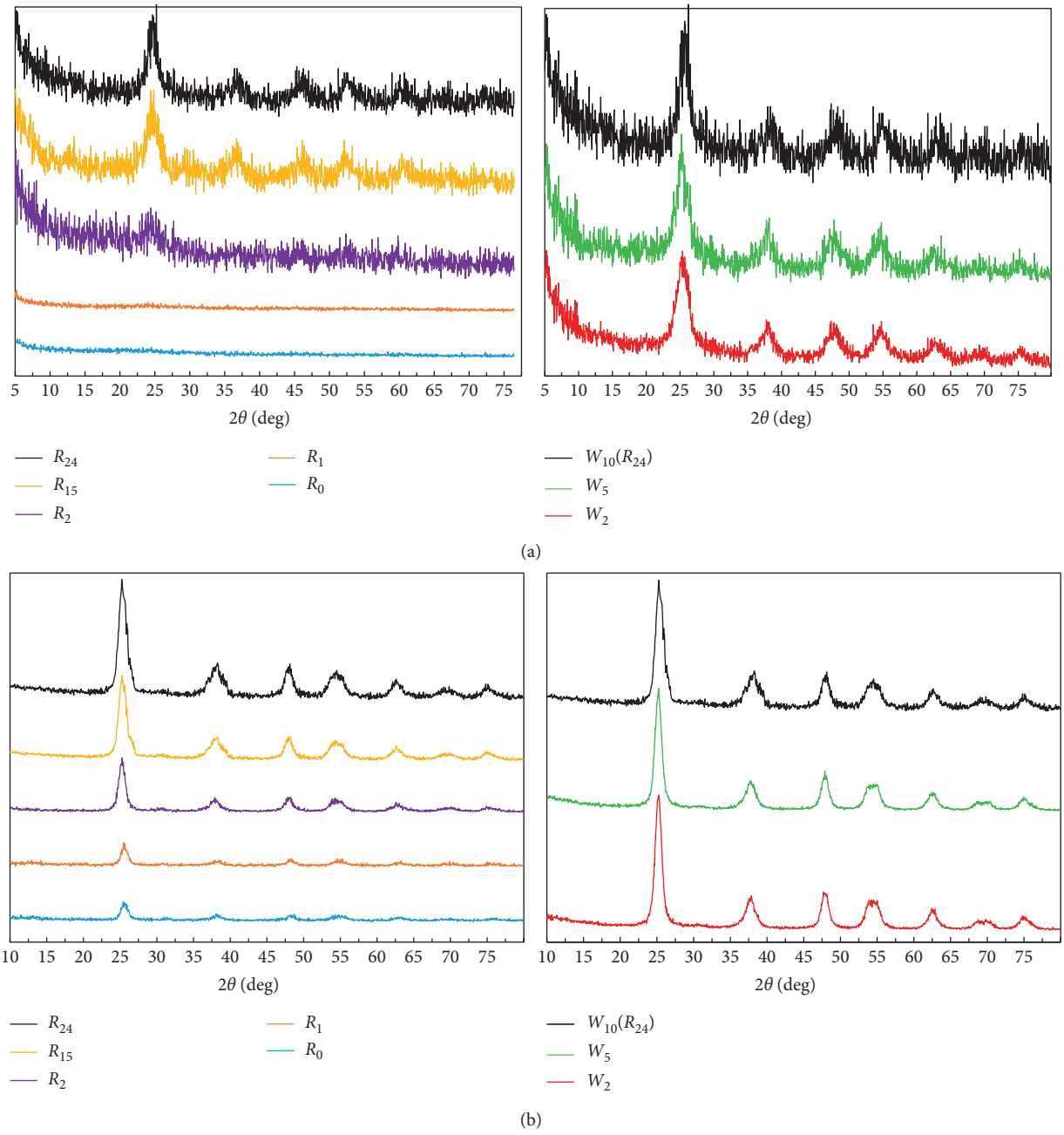

FIGURE 5: X-ray diffraction patterns of TiO_2 nanoparticles in the as-prepared state (a) and treated condition (b), obtained through different refluxing time (on the left) and different water-to-surfactant ratio (on the right).

lower density values containing organic residuals. The samples R_1 and R_2 display unique behaviors with respect to the R_0 one in most of characterization results, suggesting that, for lower reflux times, the interactions between the different phases, in organic and aqueous media, are still strong and complex.

Another conclusion derived from the reported data in Table 1 is regarding the crystallinity of as-prepared powders: more nanocrystalline anatase phase is obtained in case of increasing the reflux time, as also shown in Figure 5(a) where the XRD spectra of the as-prepared samples are reported as functions of reflux time and W ratio. All samples with 24 h refluxing time are evidently more crystalline than other samples, indicating a higher yield of the hydrolysis-condensation reactions in the micellar environment. However, in the samples of lower W ratio, a slight degradation in crystallinity and a little reduction of crystallite size are identified. This conclusion is confirmed by the TEM observation, as illustrated in Figure 4(a) for the samples R_{24} (W_{10}) and W_2 in the as-prepared condition. The TEM analysis shows that both samples are composed of ultrafine uniform spherical nanoparticles with the dimension of 5–10 nm that display the lattice fringes. The selected area electron diffraction (SAED) patterns and the corresponding indexing graphs indicate the crystallographic features of anatase phase with the interatomic spacing of $d \approx 3.7A^{\circ}$ for

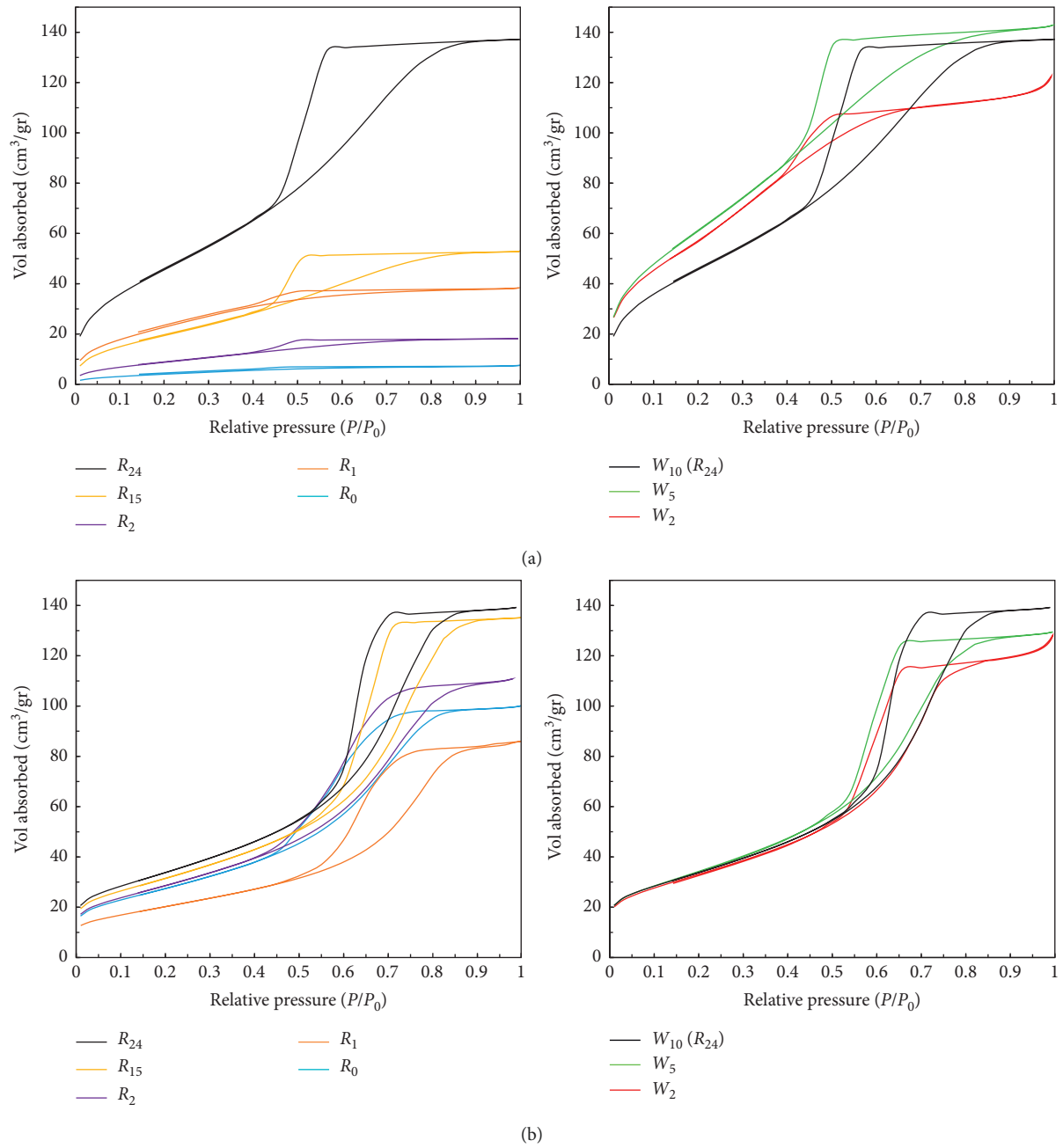

FIGURE 6: The isothermal N_2 physisorption curves of TiO_2 nanoparticles in the as-prepared state (a) and the treated condition (b), obtained through different refluxing time (on the left) and different water-to-surfactant molar ratio (on the right).

(101) planes. In accordance with XRD results, the higher W ratio is associated with increased crystallinity.

In addition to uniformity and crystallinity, enhancing the surface area and porosity features of the as-prepared samples is another goal of this work. The data reported in Table 1 indicate that both reflux time and W ratio play a key role on the obtained values for the specific surface area of as-prepared TiO_2 nanoparticles. By increasing the reflux time to 24 h, larger surface area value up to nearly 180 $m^2 \cdot g^{-1}$ is obtained which even increases to 220–240 $m^2 \cdot g^{-1}$ in case of low W ratios, much higher than the reported values for commercial catalysts based on titanium dioxide [31]. In the isothermal nitrogen physisorption curves depicted in the upper part of Figure 6(a), a plateau region at high values of relative pressure, P/P_0, is observed for all of the samples, indicating the presence of mesoporous solids. For R_0 and R_1, the adsorption branch can be classified as a composite of Type I and Type II curves, according to IUPAC classification [32], whereas R_2, R_{15}, and R_{24} samples display Type IVa isotherms. Moreover, all the curves are characterized by the presence of hysteresis loops, attributable to Type H_4 for the former samples and Type H_{2a} for the latter ones. The results concluded from the physisorption analyses can be interpreted as follows: (i) for no or short refluxing times, the gas

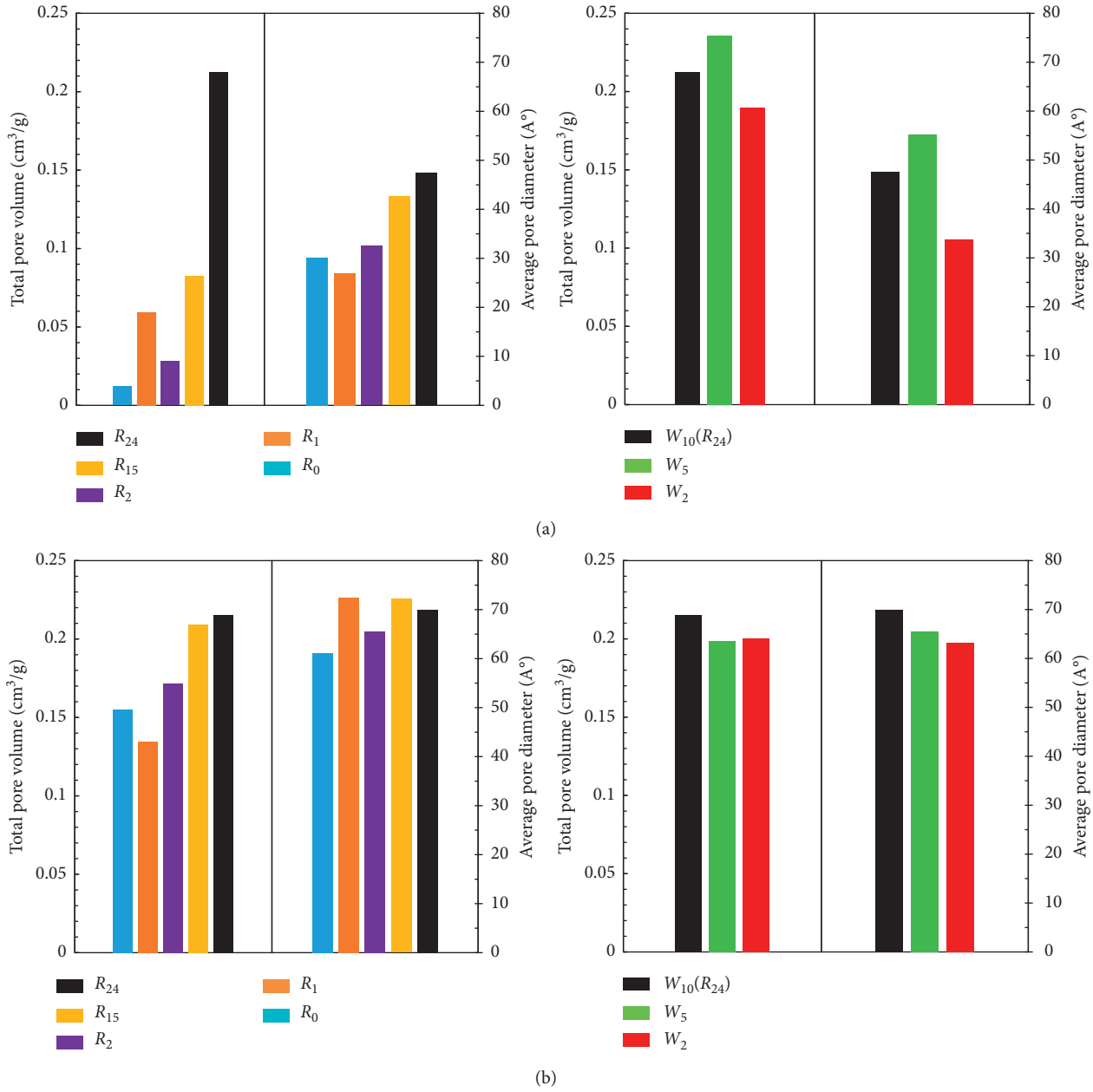

Figure 7: A comparison for the BJH Adsorption total pore volume and BJH adsorption average pore diameter of TiO_2 nanoparticles in the as-prepared state (a) and the treated condition (b), obtained through different refluxing time (on the left) and different water-to-surfactant molar ratio (on the right).

uptake can be associated with the micropore filling; (ii) for longer times, a more complex pore and network structures take place, as referred for many ordered metal oxides [33]; (iii) for a low W ratio, the plateau region is less evident, probably due to less amount of mesopores. Complementary details can be obtained through the porosity analysis of the samples in terms of the evaluation of total and average pore volume at relative pressures of $P/P_0 > 0.95$, as indicated for mesoporous solids [33], and also the distribution curves of pore volume with respect to the pore diameter obtained via the BJH method. The illustrated results in Figures 7(a) and 8(a) imply that all samples display broad pore distribution curves with a unimodal trend; however, short reflux time leads to very small pore volumes, whereas the reflux for 24 h brings about highest pore volume values, among which high to intermediate values of W ratio exhibit higher pore volumes. The observations regarding higher values of surface area and pore volume are in accordance with the previously discussed argument about the advantages of sufficient reflux time in obtaining surfactant-free nanoparticles in terms of better porosity features and surface quality.

4.2. Treated Samples. In Table 2, the reported values indicate that the reflux time and W ratio are also determining factors on the structural and morphological parameters of the

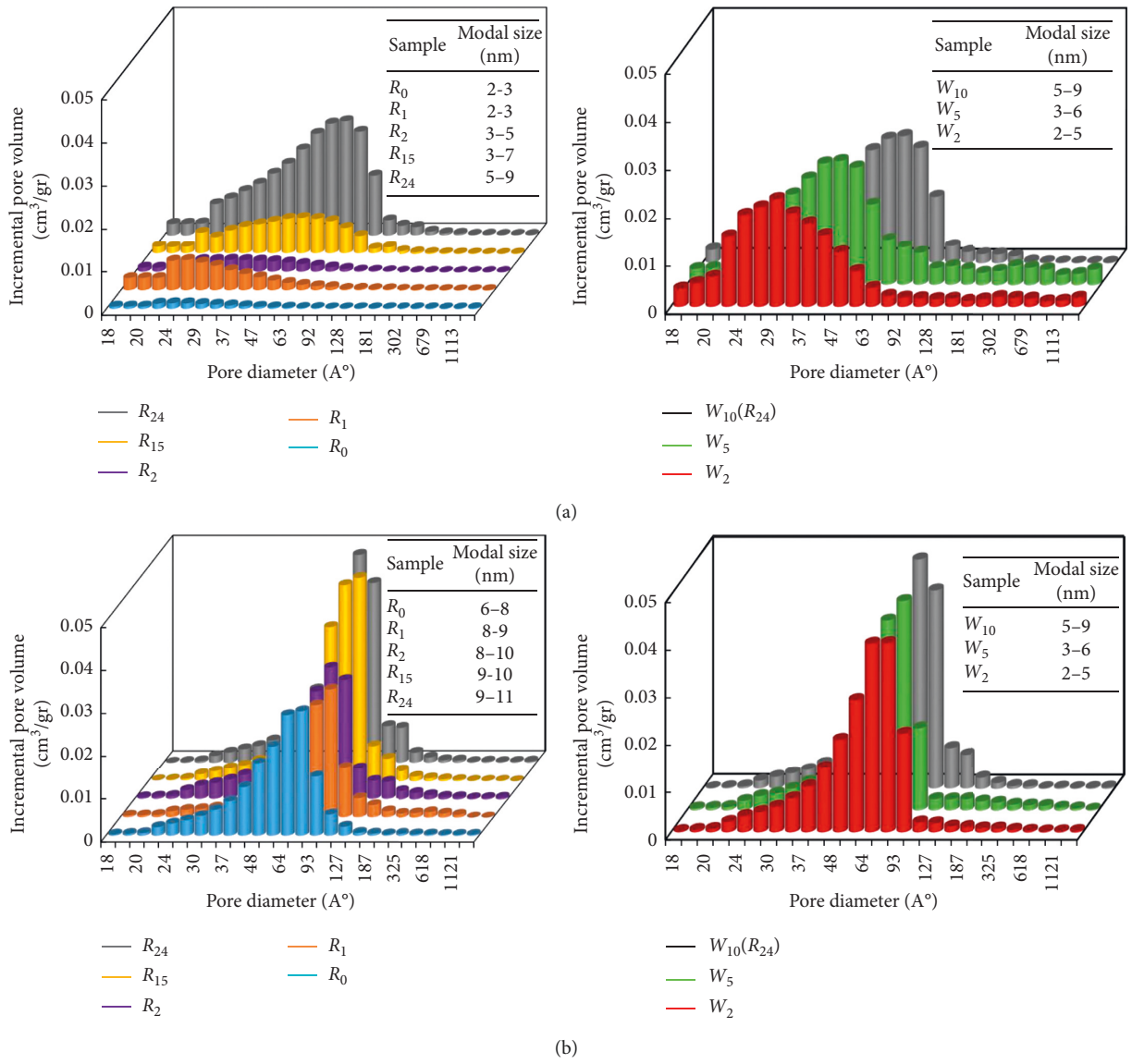

FIGURE 8: A comparison for the BJH adsorption pore size distribution of TiO_2 nanoparticles in the as-prepared state (a) and the treated condition (b), obtained through different refluxing time (on the left) and different water-to-surfactant ratio (on the right). The inset tables report the BJH adsorption modal pore diameter values, obtained from the full width at half-maximum height of the distribution curves.

treated samples, however, to a lesser extent compared to the as-prepared ones. Accordingly, the skeletal density increases and the particle size decreases with higher reflux time. Long reflux time and high to intermediate values of W ratio allow to obtain almost fully dense powders with the lowest particle size (samples R_{24} and W_5), However, even for short reflux time and low W ratio, density values of 85–90% of the theoretical limit are estimated.

Regarding the XRD spectra in Figure 5(b), the qualitative analysis evidences the presence of anatase polymorph, whereas for the samples with longer reflux time, small amounts of brookite is also implied (estimated below 4 wt%), confirming the evolution of titania nanoparticles during thermal treatment above 400°C. However, the reported values for the crystallite size in Table 2 highlight that the ordered domains of all treated samples (except R_1) fall in the narrow range of 13–15 nm, and regardless of the errors due to the simplified model adopted, crystallite size values are quite identical to the calculated particle dimensions. The same result is concluded from the TEM observation, as illustrated in Figure 4(b) for the samples R_{24} (W_{10}) and W_2 in the treated condition. In comparison with the as-prepared condition, a larger particle dimension up to 10–15 nm is observed for both samples and the lattice fringes are more evident. The selected area electron diffraction (SAED) patterns and the corresponding indexing graphs show the crystallographic features of highly crystalline anatase phase, together with a minor amount brookite phase in the samples R_{24} (the peaks marked with blue lines).

The comparison between the BET surface area and particle size value of samples before and after thermal treatment provides a useful criterion for observing the effect

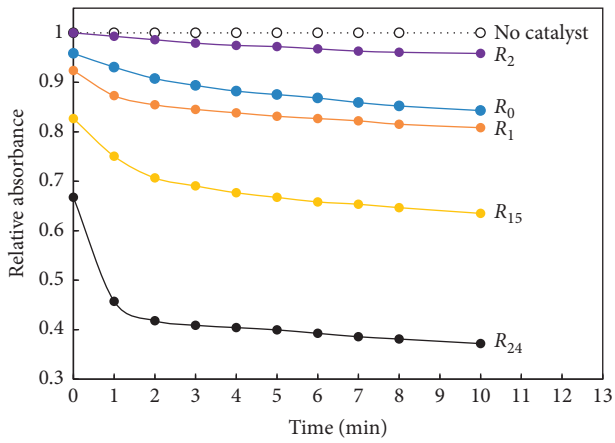

FIGURE 9: The comparison between photocatalytic activities of as-prepared TiO_2 nanoparticles in terms of relative absorbance degradation of the Calmagite dye solution over the time.

of reflux time on the obtained nanoparticle features. While the thermal treatment of R_0, R_1, R_2, and R_{15} results in higher surface area values and smaller particle sizes, opposite situation is true for all the samples prepared through 24 h reflux time. A similar trend is also observed for pore volume values since as a result of thermal treatment, the pore volume of short-refluxed samples increases while it decreases for all samples prepared through 24 h reflux time. A possible reason for such different behavior could be addressed to the low crystallinity and remaining surfactant in the former group whereby the high-temperature approach considerably improves the structural and morphological features, while for the latter group, the consequence of postcalcination process is merely the thermally activated growth of nanoparticles and surface area reduction. However, as it is reported in Table 2, in all treated samples (except R_1), the surface area values still remain high, above 100 $m^2 \cdot g^{-1}$. The physisorption curves in Figure 6(b) show that all treated samples are classified as mesoporous; however, some differences can be derived from the classification of the isothermal curves. In fact, W_2 sample displays an isothermal curve similar to those for short reflux times, whereas W_5 curve is somehow similar to that of R_{15} sample. Similar to the as-prepared powders, short reflux time leads to Type H_4 hysteresis loops, whereas R_{15}, R_{24}, W_2, and W_5 powders show Type H_{2a} loops, indicating the presence of a more complex network structures. The main discrepancy is observed for R_1 sample which displays also the lowest surface area and total pore volume values.

4.3. Photocatalytic Tests. Figure 9 provides a useful comparison between the photocatalytic activities of as-prepared nanoparticles through reporting the degradation of a UV-sensitive dye solution in terms of relative absorbance reduction over the time. The addition of R_{24} sample to the dye solution gives rise to the highest degradation rate as the absorbance decline in the form of vanishing the dye color starts immediately after the powder addition, resulting in lower absorbance value of $t = 0$ compared with those of other samples. For other samples, lower degradation rates are observed, with a trend more or less according to the specific surface area values together with crystallite size dimensions as reported in Table 1.

5. Conclusions

Mesoporous TiO_2 nanoparticles were synthesized through the surfactant-mediated sol-gel in the water-in-oil micellar system of water/cyclohexane/Triton X-100, and the effects of refluxing time and water-to-surfactant molar ratio on the on the surface area, porosity, and crystallite size of nanoparticles were studied before and after thermal treatment at 500°C. It was observed that, for the as-prepared samples, by increasing the reflux time to 24 h, the crystallinity and porosity improve considerably and the density and BET surface area increase to nearly 3.133 $g \cdot cm^{-3}$ and 180 $m^2 \cdot g^{-1}$, respectively, indicating a significant enhancement for the nanoparticles quality in anatase phase. On the other hand, for the constant reflux time of 24 h, decreasing the water-to-surfactant molar ratio from 10 to 5 and 2 leads to the formation of smaller nanoparticles with even higher surface area of around 220–240 $m^2 \cdot g^{-1}$, while a slight degradation in the crystallinity and porosity of the nanoparticles is observed. Moreover, the step for removing the surfactant from the obtained powders is considerably longer. The thermal treatment of the samples at 500°C anticipatedly contributes to an increase in the values of crystallite size and density, a narrower pore size distribution, and a reduction in surface area values; however, the surface area values of the most of the samples remain over 100 $m^2 \cdot g^{-1}$ and the particle size values do not exceed nearly 15 nm.

The obtained values indicate that reverse micelle approach is a feasible and low-cost method to synthesize TiO_2 anatase nanoparticles with high surface area and noticeable porosity features in both as-prepared and treated conditions for the applications such as photocatalysts, as confirmed by preliminary degradation tests on dye solutions; moreover, applications in the photovoltaic field can be considered as well, where the surface properties of powders result in considerable effect on the device functionality and efficiency.

Data Availability

No data were used to support this study.

Conflicts of Interest

The authors declare that there are no conflicts of interest regarding the publication of this paper.

Acknowledgments

The authors would like to acknowledge Sandra Dirè and Stefano Cristoforetti for their contribution to this work. This research was accomplished by the virtue of the PhD grant provided by the University of Trento and received no external funding.

References

[1] X. Chen and S. S. Mao, "Titanium dioxide nanomaterials: synthesis, properties, modifications, and applications," *Chemical Reviews*, vol. 107, no. 7, pp. 2891–2959, 2007.

[2] A. Fujishima, X. Zhang, and D. Tryk, "TiO_2 photocatalysis and related surface phenomena," *Surface Science Reports*, vol. 63, no. 12, pp. 515–582, 2008.

[3] S. Lee, I.-S. Cho, J. H. Lee et al., "Two-step sol–gel method-based TiO_2 nanoparticles with uniform morphology and size for efficient photo-energy conversion devices," *Chemistry of Materials*, vol. 22, no. 6, pp. 1958–1965, 2010.

[4] M. A. Behnajady, H. Eskandarloo, N. Modirshahla, and M. Shokri, "Investigation of the effect of sol-gel synthesis variables on structural and photocatalytic properties of TiO_2 nanoparticles," *Desalination*, vol. 278, no. 1–3, pp. 10–17, 2011.

[5] L. Mahoney and R. Koodali, "Versatility of evaporation-induced self-assembly (EISA) method for preparation of mesoporous TiO_2 for energy and environmental applications," *Materials*, vol. 7, no. 4, pp. 2697–2746, 2014.

[6] I. Tamiolakis, I. N. Lykakis, A. P. Katsoulidis, and G. S. Armatas, "One-pot synthesis of highly crystalline mesoporous TiO_2 nanoparticle assemblies with enhanced photocatalytic activity," *Chemical Communications*, vol. 48, no. 53, p. 6687, 2012.

[7] Z. Zhu, C. Zhu, H. Liu, Y. Wu, G. Chen, and T. Lv, "Synthesis of monodisperse colloidal TiO_2 microspheres and performance of their dye-sensitized solar cells," *Applied Surface Science*, vol. 308, pp. 301–305, 2014.

[8] M. A. Khan, M. Shaheer Akhtar, and O.-B. Yang, "Synthesis, characterization and application of sol-gel derived mesoporous TiO_2 nanoparticles for dye-sensitized solar cells," *Solar Energy*, vol. 84, no. 12, pp. 2195–2201, 2010.

[9] M. Z. Yahaya, M. Z. Abdullah, and A. A. Mohamad, "Centrifuge and storage precipitation of TiO_2 nanoparticles by the sol-gel method," *Journal of Alloys and Compounds*, vol. 651, pp. 557–564, 2015.

[10] C. Leyva-Porras, A. Toxqui-Teran, O. Vega-Becerra et al., "Low-temperature synthesis and characterization of anatase TiO_2 nanoparticles by an acid assisted sol-gel method," *Journal of Alloys and Compounds*, vol. 647, pp. 627–636, 2015.

[11] R. Rossmanith, C. K. Weiss, J. Geserick et al., "Porous anatase nanoparticles with high specific surface area prepared by miniemulsion technique," *Chemistry of Materials*, vol. 20, no. 18, pp. 5768–5780, 2008.

[12] M. P. Pileni, "Nanosized particles made in colloidal assemblies," *Langmuir*, vol. 13, no. 13, pp. 3266–3276, 1997.

[13] E. Stathatos, P. Lianos, F. Del Monte, D. Levy, and D. Tsiourvas, "formation of TiO_2 nanoparticles in reverse micelles and their deposition as thin films on glass substrates," *Langmuir*, vol. 13, no. 16, pp. 4295–4300, 1997.

[14] M.-P. Pileni, "The role of soft colloidal templates in controlling the size and shape of inorganic nanocrystals," *Nature Materials*, vol. 2, no. 3, pp. 145–150, 2003.

[15] J. Eastoe, M. J. Hollamby, and L. Hudson, "Recent advances in nanoparticle synthesis with reversed micelles," *Advances in Colloid and Interface Science*, vol. 128-130, pp. 5–15, 2006.

[16] L. Qi, "Synthesis of inorganic nanostructures in reverse micelles," in *Encyclopedia of Surface and Colloid Science*, vol. 6183–6207, 25 pages, Taylor & Francis, Abingdon, UK, 2nd edition, 2006.

[17] M. A. Malik, M. Y. Wani, and M. A. Hashim, "Microemulsion method: a novel route to synthesize organic and inorganic nanomaterials," *Arabian Journal of Chemistry*, vol. 5, no. 4, pp. 397–417, 2012.

[18] O. L. Galkina, V. V. Vinogradov, A. V. Agafonov, and A. V. Vinogradov, "Surfactant-assisted sol-gel synthesis of TiO_2 with uniform particle size distribution," *International Journal of Inorganic Chemistry*, vol. 2011, Article ID 108087, 8 pages, 2011.

[19] C. Saiwan, S. Krathong, T. Anukulprasert, and E. A. O'rear III, "Nano-titanium dioxide synthesis in AOT microemulsion system with salinity scan," *Journal of Chemical Engineering of Japan*, vol. 37, no. 2, pp. 279–285, 2004.

[20] P. D. Moran, J. R. Bartlett, J. L. Woolfrey, G. A. Bowmaker, and R. P. Cooney, "Formation and gelation of titania nanoparticles from AOT reverse micelles," *Journal of Sol-Gel Science and Technology*, vol. 8, no. 1–3, pp. 65–69, 1997.

[21] W. Cai, H. Yang, and X. Guo, "A facile synthesis of nanocrystalline spherical TiO_2 particles and its photoluminescent properties," *Procedia Engineering*, vol. 94, pp. 71–75, 2014.

[22] M. S. Lee, S. S. Park, G.-D. Lee, C.-S. Ju, and S.-S. Hong, "Synthesis of TiO_2 particles by reverse microemulsion method using nonionic surfactants with different hydrophilic and hydrophobic group and their photocatalytic activity," *Catalysis Today*, vol. 101, no. 3-4, pp. 283–290, 2005.

[23] P. Kluson, P. Kacer, T. Cajthaml, and M. Kalaji, "Preparation of titania mesoporous materials using a surfactant-mediated sol-gel method," *Journal of Materials Chemistry*, vol. 11, no. 2, pp. 644–651, 2001.

[24] R. K. Keswani, H. Ghodke, D. Sarkar, K. C. Khilar, and R. S. Srinivasa, "Room temperature synthesis of titanium dioxide nanoparticles of different phases in water in oil microemulsion," *Colloids and Surfaces A: Physicochemical and Engineering Aspects*, vol. 369, no. 1–3, pp. 75–81, 2010.

[25] R. Inaba, T. Fukahori, M. Hamamoto, and T. Ohno, "Synthesis of nanosized TiO_2 particles in reverse micelle systems and their photocatalytic activity for degradation of toluene in gas phase," *Journal of Molecular Catalysis A: Chemical*, vol. 260, no. 1-2, pp. 247–254, 2006.

[26] T. Hussain and R. Batool, "Microemulsion route for the synthesis of nano-structured catalytic materials," in *Properties and Uses of Microemulsions*, 13 pages, InTech, London, UK, 2017.

[27] R. J. Robson and E. A. Dennis, "The size, shape, and hydration of nonionic surfactant micelles. Triton X-100," *The Journal of Physical Chemistry*, vol. 81, no. 11, pp. 1075–1078, 1977.

[28] B. Ohtani, Y. Ogawa, and S. Nishimoto, "Photocatalytic activity of amorphous–anatase mixture of titanium (IV) oxide particles suspended in aqueous solutions," *The Journal of Physical Chemistry B*, vol. 101, no. 19, pp. 3746–3752, 2002.

[29] R. Zhang and L. Gao, "Preparation of nanosized titania by hydrolysis of alkoxide titanium in micelles," *Materials Research Bulletin*, vol. 37, no. 9, pp. 1659–1666, 2002.

[30] L. Lutterotti, "Total pattern fitting for the combined size-strain-stress-texture determination in thin film diffraction," *Nuclear Instruments and Methods in Physics Research Section B: Beam Interactions with Materials and Atoms*, vol. 268, no. 3-4, pp. 334–340, 2010.

[31] A. Di Paola, G. Cufalo, M. Addamo et al., "Photocatalytic activity of nanocrystalline TiO_2 (brookite, rutile and brookite-based) powders prepared by thermohydrolysis of $TiCl_4$ in aqueous chloride solutions," *Colloids and Surfaces A: Physicochemical and Engineering Aspects*, vol. 317, no. 1–3, pp. 366–376, 2008.

[32] M. Thommes, K. Kaneko, A. V. Neimark et al., "Physisorption of gases, with special reference to the evaluation of surface area

and pore size distribution (IUPAC Technical Report)," *Pure and Applied Chemistry*, vol. 87, no. 9-10, pp. 1051–1069, 2015.

[33] F. Rouquerol, J. Rouquerol, K. S. W. Sing, P. Llewellyn, and G. Maurin, *Adsorption by Powders and Porous Solid: Principles, Methodology and Applications*, pp. 429–438, Academic Press, San Diego, CA, USA, 2014.